AGU ADVANCING EARTH AND SPACE SCIENCE

Geophysical Research Letters

RESEARCH LETTER
10.1029/2020GL090864

Multisatellite Imaging of a Gas Well Blowout Enables Quantification of Total Methane Emissions

Daniel H. Cusworth[1], Riley M. Duren[1,2], Andrew K. Thorpe[1], Sudhanshu Pandey[3], Joannes D. Maasakkers[3], Ilse Aben[3], Dylan Jervis[4], Daniel J. Varon[4,5], Daniel J. Jacob[5], Cynthia A. Randles[6], Ritesh Gautam[7], Mark Omara[7], Gunnar W. Schade[8], Philip E. Dennison[9], Christian Frankenberg[10], Deborah Gordon[11], Ettore Lopinto[12], and Charles E. Miller[1]

[1]Jet Propulsion Laboratory, California Institute of Technology, Pasadena, CA, USA, [2]University of Arizona, Tucson, AZ, USA, [3]SRON Netherlands Institute for Space Research, Utrecht, The Netherlands, [4]GHGSat Inc, Montreal, Canada, [5]School of Engineering and Applied Sciences, Harvard University, Cambridge, MA, USA, [6]ExxonMobil Research and Engineering Company, Annandale, NJ, USA, [7]Environmental Defense Fund, Washington, DC, USA, [8]Department of Atmospheric Sciences, Texas A&M University, College Station, TX, USA, [9]Department of Geography, University of Utah, Salt Lake City, UT, USA, [10]Division of Geology and Planetary Sciences, California Institute of Technology, Pasadena, CA, USA, [11]Watson Institute for International and Public Affairs, Brown University, Providence, RI, USA, [12]Italian Space Agency, Rome, Italy

Key Points:

- We capture methane emission dynamics of a gas well blowout by combining observations from several satellites
- The PRISMA satellite is capable of retrieving both CO_2 and CH_4 emissions during flare combustion, allowing for an efficiency estimate
- Satellite emission estimates are validated against a bottom-up oil/gas methane emission model

Supporting Information:

- Supporting Information S1

Correspondence to:
D. H. Cusworth,
daniel.cusworth@jpl.nasa.gov

Citation:
Cusworth, D. H., Duren, R. M., Thorpe, A. K., Pandey, S., Maasakkers, J. D., Aben, I., et al. (2021). Multisatellite imaging of a gas well blowout enables quantification of total methane emissions. *Geophysical Research Letters*, *48*, e2020GL090864. https://doi.org/10.1029/2020GL090864

Received 21 SEP 2020
Accepted 19 NOV 2020

Abstract Incidents involving loss of control of oil/gas wells can result in large but variable emissions whose impact on the global methane budget is currently unknown. On November 1, 2019, a gas well blowout was reported in the Eagle Ford Shale. By combining satellite observations at different spatial and temporal scales, we quantified emissions 10 times during the 20-day event. Our multisatellite synthesis captures both the short-term dynamics and total integrated emissions of the blowout. Such detailed event characterization was previously not possible from space and difficult to do with surface measurements. We present 30-m methane and carbon dioxide plumes from the PRISMA satellite, which let us estimate flare combustion efficiency (87%). Integrating emissions across all satellites, we estimate 4,800 ± 980 metric tons lost methane. Blowouts occur across the globe and multisatellite observations can help to determine their pervasiveness, enable corrective action, and quantify their contribution to global methane budgets.

Plain Language Summary Well control loss at oil/gas wells (e.g., blowouts) can lead to methane emission releases that are difficult to quantify from the surface. New advances in satellite remote sensing can effectively capture emission dynamics when information from multiple satellites is combined. A gas well blowout was reported on November 1, 2019 in East Texas, and we were able to provide 10 distinct emission estimates during the 20-day event by combining information from multiple satellites. This information synthesis allowed us to assess variability and better quantify the total methane released to the atmosphere. Blowouts occur across the globe during oil/gas production, and multisatellite observations can help to determine their pervasiveness, enable prompt corrective action, and quantify their contribution to national and global methane budgets.

1. Introduction

The primary constituent of gas emitted from oil/natural gas infrastructure is methane (CH_4), which is the second most important anthropogenic greenhouse gas (GHG) after carbon dioxide (CO_2) based on its radiative forcing (Myhre et al., 2013). There is increasing evidence that CH_4 emissions from this infrastructure follow a heavy-tailed distribution (Duren et al., 2019; Frankenberg et al., 2016; Lyon et al., 2015; Zavala-Araiza et al., 2015). The heavy tail of the emission distribution comes from routine operational practices (e.g., well venting from liquids unloading), avoidable operating conditions, and unexpected equipment malfunctions (e.g., pipeline leaks, blowouts). Emissions from unexpected events can be difficult to quantify, as they may evade detection in remote areas for indefinite time, may be short lived, may have variable emissions during the event, and may present hazardous field conditions (e.g., fires, toxic emissions), all of which prevent fast and effective mobilization of surface or airborne measurements. Therefore, these events represent a potentially large and uncertain contribution to the global CH_4 budget. When remote sampling

of emissions from blowouts was possible, studies have shown that these events may be among the largest point source emissions on a national scale over the event duration (Conley et al., 2016; Pandey et al., 2019). This class of well control events are not uncommon occurrences, with many reported each year in Texas (RRC, 2020a). However, the same reporting protocols in Texas do not consistently exist in other jurisdictions nationally and internationally, which creates a large underlying uncertainty.

Independent detection and quantification of emissions from these events using satellite remote sensing is an avenue to close the uncertainty gap. Global tiered remote sensing systems for CH_4 event detection and quantification are now possible with recent launches of satellites with sufficient spatial resolution and coverage, temporal coverage, and targeting capabilities. For instance, from February to March 2018, a significant gas well blowout (~120 t h^{-1}) in Ohio was detected and quantified using the TROPOspheric Monitoring Instrument (TROPOMI; Pandey et al., 2019) onboard the Sentinel-5P satellite (Hu et al., 2018; Veefkind et al., 2012). TROPOMI provides atmospheric dry air column mixing ratio (XCH_4) maps with 7 × 5.5 km^2 nadir spatial resolution globally and daily in cloud-free conditions (Hu et al., 2018). Similarly, the GHGSat-D satellite, with its finer 50 m spatial resolution, detected prolonged venting (10–43 t h^{-1}) operations at a gas compressor station in Turkmenistan from June 2018 to January 2019 (Varon et al., 2019), results which were consistent with TROPOMI estimates. Airborne remote sensing surveys imaged and quantified emissions from the Aliso Canyon blowout January–February 2016 in California (20 t h^{-1}; Thorpe et al., 2020) with results consistent with airborne in situ methods for the same period (Conley et al., 2016). The Hyperion EO-1 satellite imaging spectrometer (2000–2017; Folkman et al., 2001) also imaged plumes three times during the event at 30 m spatial resolution and detected significant CH_4 emissions (Thompson et al., 2016).

Here, we focus on a discrete gas well blowout and show that with a combination of satellite observations, we are able to detect, quantify, and track emissions from this event. These instruments include TROPOMI, GHGSat-D, the Visible Infrared Imaging Radiometer Suite (VIIRS; Cao et al., 2013) instrument, and the PRecursore IperSpettrale della Missione Applicativa (PRISMA) satellite imaging spectrometer (launched March 2019; Loizzo et al., 2018). PRISMA has 30 m spatial resolution and measures backscattered solar radiances from 400 to 2500 nm at <12 nm spectral resolution, a range which includes both CO_2 and CH_4 absorption features. Previous theoretical work showed the potential for retrieving large CH_4 point sources with PRISMA (Cusworth et al., 2019). In this study, we provide evidence of this capability and show we can simultaneously retrieve column averaged CO_2 and CH_4 concentrations with high spatial resolution, derive emissions, and thus quantify the combustion efficiency of the flared blowout. This new capability has not been available with any single satellite instrument previously. When we combine data collection and analysis from PRISMA with other satellite instruments, we demonstrate an enhanced capability to resolve the evolution of the blowout, which has major implications for global monitoring of heavy-tailed emitters.

2. Event Timeline

At 02:40 (local time) on November 1, 2019, a blowout was reported at a gas well in the Eagle Ford Shale near Victoria, Texas (28.9°N, 97.6°W). The event occurred at a surface site where four horizontally drilled wells are colocated. Evacuation orders were issued soon after for residences within a 2-mile radius (Chapa, 2019). On 14 November, a cap was placed on the well and gas was diverted to an open pit where it was flared. On 20 November at 11:00, dense fluids were injected into the well, which effectively shut it in. From 2 to 12 November, the Devon Energy Corporation contracted CTEH, LLC to measure in situ volatile organic compounds (VOCs) within 5 km of the blowout at several sampling sites. Instantaneous benzene concentrations peaked at 236 ppb downwind of the blowout on 2 November. The first CTEH 24-h averaged benzene concentration was reported between 3 and 4 November as 16.5 ppb (Figure S1). The TCEQ Karnes County air quality station (located 30 km west of the blowout) recorded a much lower maximum benzene concentration of 7.9 ppb on 2 November, with levels diminishing afterward, but spiking to 4.6 ppb briefly between 14 and 15 November (Figure S1). No direct CH_4 measurements were made during in situ monitoring, but we infer CH_4 emissions based on chemical transport modeling and the gas composition of the well (Section S1). The Texas Railroad Commission (RRC) reports blowouts and well-control problems publicly and includes information regarding causes, injuries, and operators (RRC, 2020a). TCEQ maintains the Air Emission Event report system, which publishes endorsed company reports of emission events. However, neither RRC nor TCEQ have posted official reports at the time of this study's submission.

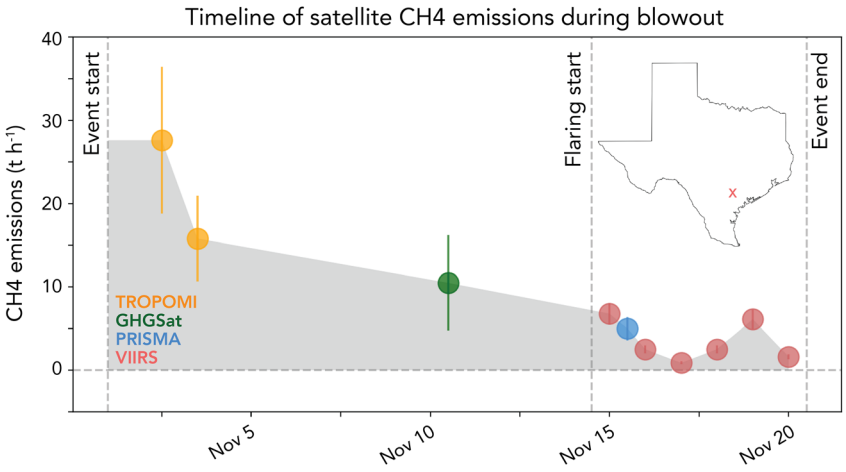

Figure 1. Timeline of satellite derived CH_4 emissions made during the blowout. PRISMA and GHGSat were specifically tasked to image the blowout. TROPOMI and VIIRS are global mappers, and we collected observations when conditions (e.g., clear skies) allow. Emission estimation is detailed in the supporting information. The gray shading represents the integral of emissions. Inset is a map of Texas, with an "x" indicating the blowout location.

From space, we retrieve XCH_4 from TROPOMI, GHGSat, and PRISMA, and XCO_2 from PRISMA, and use this information to quantify total emissions from the event. We also infer CH_4 emission rates using satellite proxies, specifically flaring radiant heat from VIIRS. Availability of satellite observations depends on favorable weather conditions (in particular clear skies), and on the revisit and sampling strategy of the instrument. In this study, we use two sampling approaches jointly to constrain the blowout. The first approach uses coarse resolution global mappers with daily revisit, which here include TROPOMI for direct XCH_4 retrieval, and VIIRS, which is used to measure nighttime gas flaring radiant heat at 750 m resolution and derive methane emission rates (Elvidge et al., 2016). The second approach uses high-resolution target instruments that must be tasked to image a particular region. For this study, we requested tasking of GHGSat-D, PRISMA, and Planet Lab's SkySat, a 70 cm four-channel red-blue-green (RGB) and near infrared (740–900 nm; Murthy et al., 2014) instrument to image the blowout. When we coordinate tasking and combine information from all instruments, we gain much more insight into the evolution of and the integral emission from the blowout.

3. Emission Estimates During the Blowout

Figure 1 shows the CH_4 emission rates derived from each measurement platform. The details of deriving emission rate estimates from each instrument are provided in the supporting information. Starting with TROPOMI, we have observations available on 2, 3, 15, and 18 November (Figure S2). The spatial resolution of TROPOMI generally limits its ability to identify individual CH_4 point sources (Cusworth et al., 2018), but recent studies have shown that for very large events like blowouts or large venting, plumes are visible at this spatial resolution (Pandey et al., 2019; Varon et al., 2019). We estimate emissions from a TROPOMI scene by simulating atmospheric transport using the Weather Research and Forecasting Chemistry (WRF-Chem) model (Powers et al., 2017). We drive an initial WRF-Chem simulation using a somewhat arbitrary emission rate and then sample the resulting simulated concentration fields at the TROPOMI spatial resolution (Section S1). We then scale the blowout enhancement from this simulation to fit the observed TROPOMI concentrations and apply this scaling to the initial WRF-Chem emission rate to estimate blowout emissions. For 2 November (Figure S2), we estimate a possible mean emission range of 18–163 t h^{-1}. This wide range is due to sparse pixel sampling from quality filtering (Figure S2) and variable meteorology on that day (Figure S3). We compare this emission estimate against another derived using the Integrated Methane Enhancement (IME) algorithm (Cusworth et al., 2019; Frankenberg et al., 2016; Varon et al., 2018). This method does not invoke a transport model but instead estimates emissions by multiplying the excess methane mass generated within a retrieved methane plume by the inverse lifetime of the plume, which is calculated from the boundary layer wind speed and plume length (Section S2). Using this method, for 2 November, we

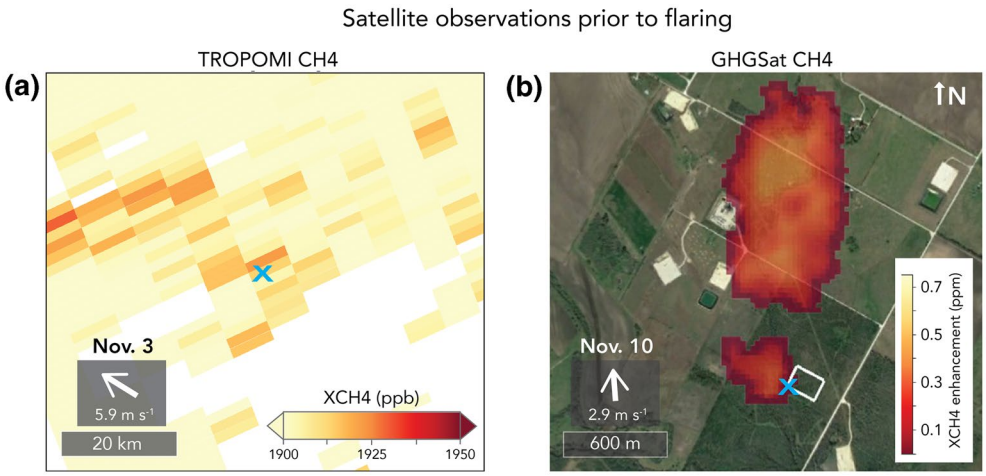

Figure 2. Satellite observations of the blowout prior to flaring. (a) TROPOMI dry air column mixing ratio of CH_4 (XCH_4) on 3 November, with the blowout location marked as "x" and the plume emanating along the southeasterly winds. (b) The GHGSat-D plume retrieved on 10 November at 50 m spatial resolution, with the plume emanating along the southerly winds. The GHGSat-D plume is overlaid on a Google Earth image, which was taken December 2018, before the well platform was built (outlined in white).

estimate an emission rate of 27.6 ± 8.8 t h^{-1} (1σ). This IME-based estimate is on the lower end of the WRF-Chem range, but consistent with bottom-up methods described later. IME methods rely on wind speed and not wind direction, which may explain the lower uncertainty for 2 November when compared to the WRF-Chem simulation. By 3 November, the IME-based emission rate dropped to 15.8 ± 5.1 t h^{-1}. Cloudy conditions persisted at the 7 km scale over the next several days, limiting additional TROPOMI scenes, and by 15 November, a discernible plume signal was lost, indicating that any remaining emissions following flaring were below the instrument's detection threshold. For subsequent calculations that integrate total CH_4 emissions over the event (see Section 4), we use the IME-based estimates for TROPOMI, given their lower uncertainty. We also set the emission rate between the blowout start and the first TROPOMI overpass to the 2 November TROPOMI estimate.

GHGSat-D imaged the blowout on 10 November at a much finer 50 × 50 m^2 effective spatial resolution. GHGSat-D has previously quantified CH_4 point sources as low as 3–4 t h^{-1} from a single overpass (Varon et al., 2019). In Figure 2, a CH_4 plume is clearly visible emanating from the blowout source and extending along the southerly winds. For emission quantification, we apply specific IME and cross-sectional flux methods tailored to the GHGSat-D instrument (Section S2; Varon et al., 2019). We estimate an emission rate of 10.5 ± 5.7 t h^{-1}, a 67% drop in emission rate from the TROPOMI IME estimate for 2 November. The reduction in emissions throughout the duration of the blowout was previously been observed in the case of the widely documented Aliso Canyon blowout (Conley et al., 2016) and here may be indicative of decreasing well pressure.

We corroborate the trend between TROPOMI and GHGSat-D emission estimates by inferring CH_4 emissions from in situ VOC measurements. Although CH_4 was not directly monitored from the ground, if we assume a fixed gas composition of the well (Table S1), we can estimate near surface CH_4 concentrations from several measured proxy VOCs (i.e., pentanes and butanes). Then, using a similar WRF-Chem setup as for comparisons to TROPOMI data, we simulate atmospheric transport to derive emission rates (Section S1). On 2 November, we estimate a CH_4 emission rate of 61 ± 32 t h^{-1}, which is higher but within the uncertainty of the TROPOMI IME-based emission estimate, and within the TROPOMI WRF-Chem emission estimate range. Wind conditions did not allow for the in situ network to adequately sample the plume on 3 and 4 November. Between 5 and 8 November, mean CH_4 emissions derived from the in situ proxies fluctuated between 6.8 and 12.6 t h^{-1}. The GHGSat-D emission rate is consistent with the range of in situ estimates, and together, they show a decreasing trend from the initial emission rate, albeit with significant variability. Though reduced, the range of 6.8–12.6 t h^{-1} still represents a very large source of methane. Only two point sources in the US EPA national Greenhouse Gas Reporting Program (a coal mine and a landfill) exceed 10 t h^{-1} routine emissions on an annual basis (Jacob et al., 2016).

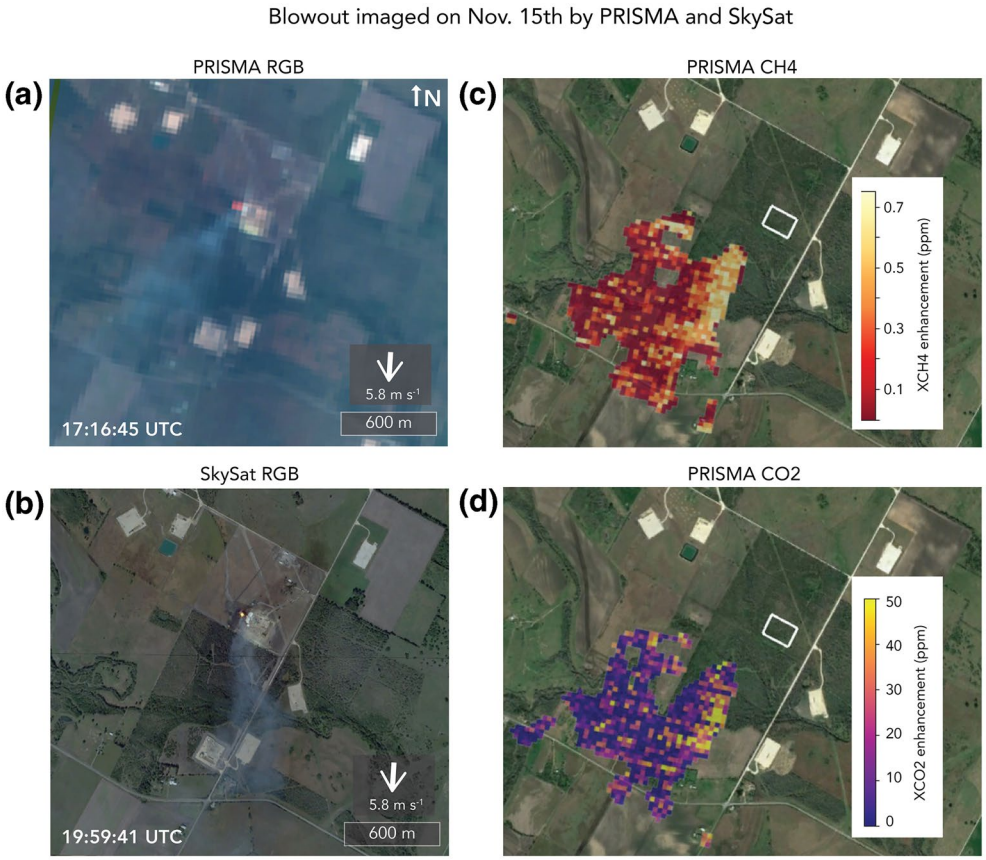

Figure 3. PRISMA and SkySat RGB images and CH_4/CO_2 plumes on 15 November, shortly after a flare had been applied to the blowout. (a, b) RGB images of the blowout from PRISMA (30 m) and SkySat (70 cm). Condensate/aerosol plumes are visible in both images. (c, d) The CH_4/CO_2 plumes retrieved from PRISMA spectra using the IMAP-DOAS retrieval algorithm (Section S4) overlaid on a Google Earth image from December 2018. The well platform is outlined in white.

On 15 November, both PRISMA and SkySat imaged the blowout within a 2-h period, after flaring had been initiated to diverted well gas. Figure 3 shows the RGB images from both PRISMA and SkySat. The large flare is visible in both images, covering four PRISMA pixels. Also visible is a large aerosol, condensate, and/or condensation plume, which extends approximately 1.5 km from the well pad, along the northerly winds. We retrieve column XCO_2 and XCH_4 by applying the Iterative Maximum A Posteriori-Differential Optical Absorption Spectroscopy (IMAP-DOAS) algorithm (Cusworth et al., 2019; Frankenberg et al., 2005; Thorpe et al., 2017) to each pixel within the scene (Section S3). We infer emission rates by applying the IME method to retrieved CH_4 and CO_2 plumes (Section S2). Retrievals near the plume source are discarded due to strong sensor saturation from scattered radiance (Pandey et al., 2019). Despite missing enhancements over the source location, we still estimate significant CO_2 and CH_4 emissions of 172 ± 71 and 5.0 ± 1.4 t h^{-1}, respectively. Assuming that the CH_4 emission came primarily from incomplete combustion, we follow the method of Caulton et al. (2014) and Gvakharia et al. (2017) and use the ratio of CH_4 to CO_2 emissions to derive an estimate for combustion efficiency (CE):

$$\mathrm{CE}(\%) = \left(1 - \frac{E_{\mathrm{CH_4}}}{\left(A \times B \times E_{\mathrm{CO_2}}\right) + E_{\mathrm{CH_4}}}\right) \times 100 \quad (1)$$

where E represents the emission rates of CH_4 and CO_2, A is the carbon composition of methane in the well gas (based on Table S1), and B is a constant relating the molar mass of CO_2 and CH_4. Applying Equation 1 with PRISMA, we estimate 87% ± 4.0% combustion efficiency for the flare. The uncertainty of this estimate

represents the 1σ spread of CE when taking into account the uncertainties in E_{CH4}, E_{CO_2}, and A. This combustion efficiency estimate is lower than what is reported as typical flare operations (98%; US Environmental Protection Agency, 2015). However, field studies have shown that although combustion efficiency for typical gas operations in some regions may center on 98%, efficiency also follows a right-skewed distribution, meaning many conventional flares operate below 98% (Gvakharia et al., 2017).

We can go a step further and quantify flare temperature using PRISMA flare pixels, which serves as a qualitative check on flare combustion efficiency derived in Equation 1. Temperature retrievals from imaging spectrometers can be performed using mixture models that separate contributions from reflected solar and flare-emitted radiance (Dennison et al., 2006). We do this through a clustering of nonflared pixel spectra into representative background endmembers and combining with MODTRAN emitted radiance simulations over a range of plausible flare temperatures (Section S4). Applying these methods to PRISMA pixels where flaring is visibly apparent (Figure 3), we retrieve temperatures from 1650 to 1800 K (Figure S7). The PRISMA retrieved temperatures are within the normal oil/gas operational range of flare temperatures (Elvidge et al., 2016), although as previously mentioned, our 87% combustion efficiency estimate is below typical flaring operations (98%). Operator efforts to control the well allowed for large amounts of gas to be flared, which can explain the high retrieved PRISMA temperatures. However, gas diversion to an open pit, though ultimately successful in helping regain well control, may have led to some gas to escape unflared, leading to lower than normal combustion efficiency for typical flare operations.

VIIRS can be used to retrieve radiant heat, which is related to the volumetric quantity of flared gas (Elvidge et al., 2016). If flare combustion efficiency is known, this relationship between VIIRS radiant heat and the flared gas quantity can be used to estimate noncombusted CH_4 emissions (Section S5). VIIRS retrieved a flare temperature of 1,585–1,615 K during its nighttime overpass on 15 November, which is slightly lower than the 1,650–1,800 K temperature range retrieved during the day from PRISMA. However, PRISMA temperature falls broadly within the VIIRS temperature range over the entirety of flaring from 15 to 20 November (1,470–2,170 K). Therefore, we take the 87% ± 4.0% combustion efficiency derived from PRISMA and apply it to VIIRS radiant heat retrievals to estimate CH_4 emission rates. On 15 November, we estimate CH_4 emissions of 6.8 ± 1.3 t h^{-1} from VIIRS, which is higher, but consistent within the uncertainties of the PRISMA estimate. The flare and subsequently the well were shut-in on 20 November. The VIIRS emission rate for 20 November prior to the shut-in was 1.6 ± 0.3 t h^{-1}. Though this is still significant, it represents a small fraction of peak emissions from the blowout. We have no additional emission constraints after the twentieth, so are unable to determine if any residual emissions were present after the blowout. We assume that emissions associated with the event ended after 20 November.

4. Discussion

Combining multiple satellite and in situ emission estimates for individual days allows us to estimate the total gas lost during the blowout event. Integrating satellite emission rates, we estimate 4,830 ± 980 metric tons of CH_4 were lost to the atmosphere. Therefore, with effective combination of multisensor satellites aided by favorable meteorological conditions, this work shows a clear path forward for quantifying CH_4 emissions from blowouts entirely from space. In the present analysis, no one satellite was able to capture all the dynamics of the blowout, due to observational factors including spatial resolution, spatial coverage, and target revisit frequency, as well as region-specific issues including cloud cover and the presence of flaring. Only after coordinated targeting and multisensor analysis were we able to more accurately constrain the emissions.

We compare our top-down emission estimates with a bottom-up lifecycle analysis from the Oil-Climate Index (OCI) model (Brandt et al., 2018; Gordon et al., 2015). The OCI model estimates upstream GHG emissions, gas at the well, and fugitive methane loss rate at the well level using field depth, well dimension, well pressure, gas-to-oil ratio, and liquids gravity, among other inputs (Table S2). To model a blowout with OCI, we use reported reservoir actuation pressures, as these represent pressures that the hydraulic fracturing process must overcome to produce gas (see Section S6). Though an official report of this event is not yet available (RRC, 2020a), RRC reports four horizontally drilled gas wells on the Devon Migura Lease that were directionally drilled from the same surface location where the blowout occurred (RRC, 2020c). These wells had successive spud dates dated between 30 April 2019 and 9 May 2019, several months before

the blowout occurred (RRC, 2020b). The existence of pressure communication between adjacent wells and reservoirs has been shown to exist in the Eagle Ford Shale under fracture treatment (Sukumar et al., 2019). Given that the four horizontal gas wells (1H, 2H, 5H, and 6H) have the same surface location where the blowout occurred (Figure S8), we assume well communication and model CH_4 emissions using actuation pressure assumptions (Table S2). With OCI, we estimate 22.4 t h^{-1} maximum emission rate associated with the blowout, consistent with the TROPOMI 2 November overpass.

We simulate daily bottom-up emissions using OCI during the blowout (Table S4). Daily emission changes are driven by applying operational information (e.g., specific time blowout started and flaring was applied) and ancillary atmospheric observations (e.g., trends in VOCs). Table S4 compares the top-down emission time series with OCI daily estimates and shows close correspondence. OCI total methane over the 20-day course of the blowout event is estimated at 4,630 metric tons, consistent with the satellite estimate. Finally, OCI estimates that under normal operating conditions, the four wells involved in this blowout together would have emitted 66 metric tons of fugitive methane in total over the course of 20 days, using an average leakage rate of 0.012 kg CH_4 per kg CH_4 at the wellbore (Table S3). Therefore, the blowout is estimated by OCI to have increased CH_4 emissions from the wells involved by a factor of 75 over routine operations.

Blowouts represent a potentially large global GHG source, but their emissions are poorly understood. In Texas, blowouts are required to be reported to the RRC, and all such events from 1960 to present are logged (Figure S9; RRC, 2020c). Since the 1980s, flared and unflared blowouts in Texas have decreased, but they are still frequent today. Globally, there is much less open-access information about blowout statistics, so we lack bottom-up constraints to quantify the contributions to the anthropogenic CH_4 budget. Satellites will be critical to closing this uncertainty gap. Similarly, satellites could be key to identify and quantify methane emissions from other unexpected events (e.g., unlit flares in remote regions, underground pipelines, and failed controls on elevated point sources). The GeoCARB mission will extend TROPOMI's capability by providing daily CH_4 maps across North and South American land masses at 5–10 km resolution (Moore et al., 2018), and the MethaneSAT mission is planned to provide ~1 km CH_4 maps focusing on major oil/gas basins globally at least weekly (Wofsy & Hamburg, 2019). GHGSat is planning on expanding its observing capacity with two additional instruments, GHGSat-C1 (launched 2020) and GHGSat-C2 (expected launch 2021; Jervis et al., 2020). Many imaging spectrometers with targeting capabilities similar to PRISMA with similar or better spectral resolution and signal-to-noise are set to launch in the next few years (EnMAP, Guanter et al., 2015; EMIT, Green et al., 2018). Globally mapping imaging spectrometers with 10–15 days revisit cycles are also planned to launch in the next decade (SBG, Hochberg et al., 2015; CHIME, Nieke, & Rast, 2018). Even with these new observing platforms, constraining all the dynamics of large emission events will require coordinated tasking and combining of all satellite information. As we showed with PRISMA, these instruments will have the ability to map both CH_4 and CO_2 plumes, and comparison of the corresponding emission rate estimates allowed us to assess CH_4 combustion efficiency. This confirms previous theoretical work that has indicated the possibility of doing CH_4 monitoring with spaceborne imaging spectrometers (Ayasse et al., 2019; Cusworth et al., 2019). Using the visible and near infrared PRISMA channels, we can also retrieve flare temperature, which can be an ancillary check on combustion efficiency. The ability to quantify CH_4 emissions, CO_2 emissions, flare temperature, and combustion efficiency from one satellite instrument is a new opportunity in satellite remote sensing that will greatly improve total carbon footprint accounting.

Acknowledgments
The authors thank Mike Smith at the Devon Energy Corporation for providing operator information and insights regarding this blowout event. Portions of this work were undertaken at the Jet Propulsion Laboratory, California Institute of Technology, under contract with NASA. Some of the work was supported by NASA's Carbon Monitoring System program. This research contains Copernicus Sentinel data 2019. S. Pandey is supported through the GALES (Gas LEaks from Space) project (Grant 15597) by the Dutch Technology Foundation, which is part of the Netherlands Organisation for Scientific Research (NWO). WRF simulations were carried out on the Dutch National supercomputer Cartesius maintained by SurfSara (www.surfsara.nl). The authors thank colleagues at Planet Labs for tasking SkySat in response to this event.

Data Availability Statement

TROPOMI data are available at https://s5phub.copernicus.eu/dhus/#/home. WRF-CHEM model code is available at https://ruc.noaa.gov/wrf/wrf-chem/. PRISMA data are publicly available to registered users at https://prisma.asi.it/. Registration is free and can be obtained at https://prismauserregistration.asi.it/. VIIRS data are available at https://doi.org/10.5067/VIIRS/VJ103IMG.002.

References

Ayasse, A. K., Dennison, P. E., Foote, M., Thorpe, A. K., Joshi, S., Green, R. O., et al. (2019). Methane mapping with future satellite imaging spectrometers. *Remote Sensing*, *11*, 3054.

Brandt, A. R., Masnadi, M. S., Englander, J. G., Koomey, J., & Gordon, D. (2018). Climate-wise choices in a world of oil abundance. *Environmental Research Letters*, *13*, 044027. https://doi.org/10.1088/1748-9326/aaae76

Cao, C., Xiong, J., Blonski, S., Liu, Q., Uprety, S., Shao, X., et al. (2013). Suomi NPP VIIRS sensor data record verification, validation, and long-term performance monitoring. *Journal of Geophysical Research: Atmospheres*, *118*, 11664–11678. https://doi.org/10.1002/2013JD020418

Caulton, D. R., Shepson, P. B., Cambaliza, M. O. L., McCabe, D., Baum, E., & Stirm, B. H. (2014). Methane destruction efficiency of natural gas flares associated with shale formation wells. *Environmental Science & Technology*, *48*, 9548–9554. https://doi.org/10.1021/es500511w

Chapa, S. (2019). Majority of families return home weeks after DeWitt County blowout. *Houston Chronicle*. Last Accessed June 10, 2020. Retrieved from https://www.chron.com/business/energy/article/Majority-of-families-return-home-weeks-after-14848869.php

Conley, S., Franco, G., Faloona, I., Blake, D. R., Peischl, J., & Ryerson, T. B. (2016). Methane emissions from the 2015 Aliso Canyon blowout in Los Angeles, CA. *Science*, *351*, 1317–1320. https://doi.org/10.1126/science.aaf2348

Cusworth, D. H., Jacob, D. J., Sheng, J.-X., Benmergui, J., Turner, A. J., Brandman, J., et al. (2018). Detecting high-emitting methane sources in oil/gas fields using satellite observations. *Atmospheric Chemistry and Physics*, *18*, 16885–16896. https://doi.org/10.5194/acp-18-16885-2018

Cusworth, D. H., Jacob, D. J., Varon, D. J., Chan Miller, C., Liu, X., Chance, K., et al. (2019). Potential of next-generation imaging spectrometers to detect and quantify methane point sources from space. *Atmospheric Measurement Techniques*, *12*, 5655–5668. https://doi.org/10.5194/amt-12-5655-2019

Dennison, P. E., Charoensiri, K., Roberts, D. A., Peterson, S. H., & Green, R. O. (2006). Wildfire temperature and land cover modeling using hyperspectral data. *Remote Sensing of Environment*, *100*, 212–222. https://doi.org/10.1016/j.rse.2005.10.007

Duren, R. M., Thorpe, A. K., Foster, K. T., Rafiq, T., Hopkins, F. M., Yadav, V., et al. (2019). California's methane super-emitters. *Nature*, *575*, 180–184. https://doi.org/10.1038/s41586-019-1720-3

Elvidge, C. D., Zhizhin, M., Baugh, K., Hsu, F.-C., & Ghosh, T. (2016). Methods for global survey of natural gas flaring from visible infrared imaging radiometer suite data. *Energies*, *9*, 14. https://doi.org/10.3390/en9010014

Folkman, M. A., Pearlman, J., Liao, L. B., & Jarecke, P. J. (2001). EO-1/Hyperion hyperspectral imager design, development, characterization, and calibration. In W. L. Smith & Y. Yasuoka (Eds.), Hyperspectral remote sensing of the land and atmosphere (Vol. *4151*, pp. 40–51). International Society for Optics and Photonics, SPIE. https://doi.org/10.1117/12.417022

Frankenberg, C., Platt, U., & Wagner, T. (2005). Iterative maximum a posteriori (IMAP)-DOAS for retrieval of strongly absorbing trace gases: Model studies for CH4 and CO_2 retrieval from near infrared spectra of SCIAMACHY onboard ENVISAT. *Atmospheric Chemistry and Physics*, *5*, 9–22.

Frankenberg, C., Thorpe, A. K., Thompson, D. R., Hulley, G., Kort, E. A., Vance, N., et al. (2016). Airborne methane remote measurements reveal heavy-tail flux distribution in Four Corners region. *Proceedings of the National Academy of Sciences*, *113*, 9734–9739. https://doi.org/10.1073/pnas.1605617113

Gordon, D., Brandt, A. R., Bergerson, J., & Koomey, J. (2015). *Know your oil: Creating a global oil-climate index*. Washington, DC: Carnegie Endowment for International Peace.

Green, R., Mahowald, N., Clark, R., Ehlmann, B., Ginoux, P., Kalashnikova, O., et al. (2018). *NASA's Earth surface mineral dust source investigation* AGU Fall Meeting Abstracts.

Guanter, L., Kaufmann, H., Segl, K., Foerster, S., Rogass, C., Chabrillat, S., et al. (2015). The EnMAP spaceborne imaging spectroscopy mission for Earth observation. *Remote Sensing*, *7*, 8830–8857. https://doi.org/10.3390/rs70708830

Gvakharia, A., Kort, E. A., Brandt, A., Peischl, J., Ryerson, T. B., Schwarz, J. P., et al. (2017). Methane, black carbon, and ethane emissions from natural gas flares in the Bakken Shale, North Dakota. *Environmental Science & Technology*, *51*, 5317–5325. https://doi.org/10.1021/acs.est.6b05183

Hochberg, E. J., Roberts, D. A., Dennison, P. E., & Hulley, G. C. (2015). Special issue on the Hyperspectral Infrared Imager (HyspIRI): Emerging science in terrestrial and aquatic ecology, radiation balance and hazards. *Remote Sensing of Environment*, *167*, 1–5. https://doi.org/10.1016/j.rse.2015.06.011

Hu, H., Landgraf, J., Detmers, R., Borsdorff, T., Aan de Brugh, J., Aben, I., et al. (2018). Toward global mapping of methane with TROPOMI: First results and intersatellite comparison to GOSAT. *Geophysical Research Letters*, *45*, 3682–3689. https://doi.org/10.1002/2018GL077259

Jacob, D. J., Turner, A. J., Maasakkers, J. D., Sheng, J., Sun, K., Liu, X., et al. (2016). Satellite observations of atmospheric methane and their value for quantifying methane emissions. *Atmospheric Chemistry and Physics*, *16*, 14371–14396. https://doi.org/10.5194/acp-16-14371-2016

Jervis, D., McKeever, J., Durak, B. O. A., Sloan, J. J., Gains, D., Varon, D. J., et al. (2020). The GHGSat-D imaging spectrometer. *Atmospheric Measurement Techniques Discussions*. https://doi.org/10.5194/amt-2020-301

Loizzo, R., Guarini, R., Longo, F., Scopa, T., Formaro, R., Facchinetti, C., & Varacalli, G. (2018). Prisma: The Italian Hyperspectral Mission. In *IGARSS 2018—2018 IEEE international geoscience and remote sensing symposium* (pp. 175–178). Institute of Electrical and Electronics Engineers (IEEE).

Lyon, D. R., Zavala-Araiza, D., Alvarez, R. A., Harriss, R., Palacios, V., Lan, X., et al. (2015). Constructing a spatially resolved methane emission inventory for the Barnett Shale region. *Environmental Science & Technology*, *49*, 8147–8157. https://doi.org/10.1021/es506359c

Moore, B., III, Crowell, S. M. R., Rayner, P. J., Kumer, J., O'Dell, C. W., O'Brien, D., et al. (2018). The potential of the Geostationary Carbon Cycle Observatory (GeoCarb) to provide multi-scale constraints on the carbon cycle in the Americas. *Frontiers in Environmental Science*, *6*, 109. https://doi.org/10.3389/fenvs.2018.00109

Murthy, K., Shearn, M., Smiley, B. D., Chau, A. H., Levine, J., Robinson, M. D., & Shimoda (2014). SkySat-1: Very high-resolution imagery from a small satellite. In R. Meynart, S. P. Neeck, & H. Shimoda (Eds.), Sensors, systems, and next-generation Satellites XVIII (Vol. *9241*, pp. 367–378). International Society for Optics and Photonics SPIE. https://doi.org/10.1117/12.2074163

Myhre, G., Shindell, D., Breon, F., Collins, W., Fuglestvedt, J., Huang, J., et al. (2013). *Anthropogenic and natural radiative forcing,* book section (Vol. 8). Cambridge, New York, NY: Cambridge University Press. https://doi.org/10.1017/CBO9781107415324.018

Nieke, J., & Rast, M. (2018). Toward the Copernicus Hyperspectral Imaging Mission for the Environment (CHIME). In *IGARSS 2018—2018 IEEE international geoscience and remote sensing symposium* (pp. 157–159). Institute of Electrical and Electronics Engineers (IEEE).

Pandey, S., Gautam, R., Houweling, S., van der Gon, H. D., Sadavarte, P., Borsdorff, T., et al. (2019). Satellite observations reveal extreme methane leakage from a natural gas well blowout. *Proceedings of the National Academy of Sciences*, *116*, 26376–26381. https://doi.org/10.1073/pnas.1908712116

Powers, J. G., Klemp, J. B., Skamarock, W. C., Davis, C. A., Dudhia, J., Gill, D. O., et al. (2017). The weather research and forecasting model: Overview, system efforts, and future directions. *Bulletin of the American Meteorological Society*, *98*, 1717–1737. https://doi.org/10.1175/BAMS-D-15-00308.1

RRC (2020a). Texas Railroad Commission, blowouts and well control problems. Last Accessed June 10, 2020. Retrieved from https://www.rrc.state.tx.us/oil-gas/compliance-enforcement/blowouts-and-well-control-problems/

RRC (2020b). Texas Railroad Commission, "gas well back pressure test, completion or recompletion report and log," Form G-1, May 14–18, 2020. Tracking Nos. 23299, 23330, 233317, 2332246.

RRC (2020c). Texas Railroad Commission, GIS identify results—Well location attributes. Last Accessed June 15, 2020. Retrieved from http://gis.rrc.texas.gov/GISViewer/index.html?api=12334711

Sukumar, S., Weijermars, R., Alves, I., & Noynaert, S. (2019). Analysis of pressure communication between the Austin Chalk and Eagle Ford reservoirs during a zipper fracturing operation. *Energies*, *12*, 1469.

Thompson, D. R., Thorpe, A. K., Frankenberg, C., Green, R. O., Duren, R., Guanter, L., et al. (2016). Space-based remote imaging spectroscopy of the Aliso Canyon CH_4 superemitter. *Geophysical Research Letters*, *43*, 6571–6578. https://doi.org/10.1002/2016GL069079

Thorpe, A. K., Duren, R. M., Conley, S., Prasad, K. R., Bue, B. D., Yadav, V., et al. (2020). Methane emissions from underground gas storage in California. *Environmental Research Letters*, *15*, 045005. https://doi.org/10.1088/1748-9326/ab751d

Thorpe, A. K., Frankenberg, C., Thompson, D. R., Duren, R. M., Aubrey, A. D., Bue, B. D., et al. (2017). Airborne DOAS retrievals of methane, carbon dioxide, and water vapor concentrations at high spatial resolution: Application to AVIRIS-NG. *Atmospheric Measurement Techniques*, *10*, 3833–3850. https://doi.org/10.5194/amt-10-3833-2017

US Environmental Protection Agency. (2015). *Compilation of air pollution emission factors, AP-42. Chapter 13.5* Research Triangle Park, NC: US Environmental Protection Agency, Office of Air Quality Planning and Standards. Updated April 2015. Last accessed October 27, 2020. Retrieved from https://www3.epa.gov/ttn/chief/ap42/ch13/index.html

Varon, D. J., Jacob, D. J., McKeever, J., Jervis, D., Durak, B. O. A., Xia, Y., & Huang, Y. (2018). Quantifying methane point sources from fine-scale satellite observations of atmospheric methane plumes. *Atmospheric Measurement Techniques*, *11*, 5673–5686. https://doi.org/10.5194/amt-11-5673-2018

Varon, D. J., McKeever, J., Jervis, D., Maasakkers, J. D., Pandey, S., Houweling, S., et al. (2019). Satellite discovery of anomalously large methane point sources from oil/gas production. *Geophysical Research Letters*, *46*, 13507–13516. https://doi.org/10.1029/2019GL083798

Veefkind, J., Aben, I., McMullan, K., Förster, H., De Vries, J., Otter, G., et al., et al. (2012). TROPOMI on the ESA Sentinel-5 Precursor: A GMES mission for global observations of the atmospheric composition for climate, air quality and ozone layer applications. *Remote Sensing of Environment*, *120*, 70–83.

Wofsy, S. C., & Hamburg, S. (2019). MethaneSAT—A new observing platform for high resolution measurements of methane and carbon dioxide. *AGU Fall Meeting 2019*, *A53F–02*.

Zavala-Araiza, D., Lyon, D., Alvarez, R. A., Palacios, V., Harriss, R., Lan, X., et al. (2015). Toward a functional definition of methane super-emitters: Application to natural gas production sites. *Environmental Science & Technology*, *49*, 8167–8174. https://doi.org/10.1021/acs.est.5b00133